

www.acsaem.org Article

# Polymer—Ceramic Composite Electrolytes for Lithium Batteries: A Comparison between the Single-Ion-Conducting Polymer Matrix and Its Counterpart

Laura C. Merrill, Xi Chelsea Chen,\* Yiman Zhang, Hunter O. Ford, Kun Lou, Yubin Zhang, Guang Yang, Yangyang Wang, Yan Wang, Jennifer L. Schaefer, and Nancy J. Dudney



Cite This: ACS Appl. Energy Mater. 2020, 3, 8871-8881



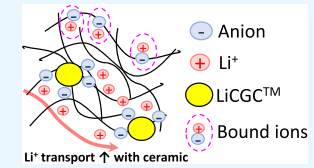
ACCESS

Metrics & More

Article Recommendations

s Supporting Information

**ABSTRACT:** Single-ion-conducting polymer electrolytes are attractive to use in lithium batteries as the transference number of the lithium cation approaches unity. This helps prevent concentration gradients across the electrolyte, which can result in dendrite formation. The addition of ceramic particles to polymer electrolytes at high loadings can increase the mechanical strength of the polymer, which can also help suppress dendrite formation. Here, a single-ion-conducting polymer electrolyte is blended with lithium-conducting oxide ceramic particles to make a composite electrolyte. This electrolyte is studied in comparison to a composite electrolyte containing freely dissolved lithium salt.



It is found that the addition of ceramic particles to the single-ion-conducting polymer can result in increased cation dissociation and consequent increased ionic conductivity. The electrolytes are cycled in lithium symmetrical cells, and it is found that the ceramic-containing electrolytes show increased interfacial stability with the lithium metal compared to the pristine polymer electrolytes. Our findings shed light on how to optimize the polymer host chemistry to form composite electrolytes that can meet the challenging requirements to stabilize the lithium metal anode.

KEYWORDS: composite, polymer, ceramic, lithium, battery, single-ion conducting, electrolyte

## 1. INTRODUCTION

With increasing demands of high-performance electronic devices and for widespread vehicle electrification, new battery chemistries with a focus on increased safety are under investigation. Lithium metal has a very high theoretical capacity compared to graphite (3800 versus 370 mAh/g) but suffers from uneven deposition causing dendrites. Dendrite formation may lead to short circuiting and subsequent fires due to the use of flammable organic solvents within the electrolyte. Solid-state electrolytes are promising in preventing dendrite growth and enabling the lithium metal anode.

Solid electrolytes encompass two classes of materials, ceramic and polymer electrolytes. Ceramic electrolytes have high mechanical moduli that can suppress dendrite growth and sufficient ionic conductivities that can reach comparable values to liquid electrolytes. What is more, most ceramics are singleion conductors. However, cracking, grain boundary resistances, stability against lithium, and the lack of processability limit the usage of ceramic electrolytes.

Polymer electrolytes are flexible, which can accommodate volume changes and prevent cracking, and have increased stability against lithium metal. Standard polymer electrolytes consist of a base polymer such as poly(ethylene oxide) (PEO) and a lithium salt dissolved in it. In polymer electrolytes, Li<sup>+</sup> movement is usually coupled to the segmental motion of the polymer chains.<sup>3</sup> Therefore, they have relatively low room-temperature ionic conductivities (<10<sup>-5</sup> S/cm).<sup>4,5</sup> Like liquid

electrolytes, the Li<sup>+</sup> transference numbers of common polymer electrolytes are low, between 0.2 and 0.5.<sup>6,7</sup> The low transference number causes concentration gradients at high current densities and leads to lithium dendrite growth.

Single-ion-conducting (SIC) polymer electrolytes, on the other hand, employ ion-containing monomers to form the polymer electrolytes. In an SIC polymer, the anions are covalently bound to the polymer chains and the Li+ transference number approaches unity. 5,6,8-12 The high transference number will prevent concentration gradients across the electrolyte and promote uniform lithium stripping and plating.<sup>6</sup> Despite the positive attributes of SIC polymers, they are intrinsically limited by low ionic conductivities. Although a lower total ionic conductivity of the SIC electrolyte is expected due to the immobilization of the anion, the conductivity of the electrolyte is often related to the ability of the cation to dissociate from the anion. 9,12,13 Single-ion conductors have also been employed as an artificial SEI as the near-unity lithium transference number prevents the anion from decomposing at the surface of the lithium metal. 14-16

Received: June 10, 2020 Accepted: August 21, 2020 Published: September 16, 2020





Thus far, research in single-ion conductors often focuses on the use of highly delocalized anions and/or engineering high ionic transport rate channels to achieve adequate ionic conductivities.  $^{6,9,10,13,17}$ 

Composite polymer electrolytes, composed of ceramic particles dispersed in a polymer matrix, may combine the advantages of ceramic and polymer to create a highly conductive, mechanically robust, and easily manufacturable solid electrolyte. The field of composite electrolytes has been under intense research in recent years. The conductivity of a composite polymer electrolyte has been shown to increase compared to that of the pristine polymer electrolyte with low ceramic loadings (<10 vol %).4,5,18-22 The proposed mechanisms for the conductivity enhancement include suppression of crystallization and enhancement of segmental dynamics of the polymer around the filler, changes in the Li<sup>+</sup>polymer complexation, and enhanced surface transport. 4-6,23-29 Furthermore, defects within the crystal lattice of the nanoparticle may cause lithium ions to enter the polymeric phase, effectively increasing the number of charge carriers contributing to the measured conductivty.<sup>21</sup>

With higher loadings of ceramic (>30 vol %), composite electrolytes with discrete ceramic fillers show greatly decreased ionic conductivity compared to the neat polymer electrolyte. Our recent studies revealed a large interfacial resistance for ion transport across the polymer—ceramic interface. Furthermore, quasi-elastic neutron scattering and solid-state nuclear magnetic resonance results demonstrated the negative impacts of a model lithium aluminum titanium phosphate (LATP) ceramic on the ionic conductivity of the polymer electrolyte. The negative impacts originated from unoptimized ceramic—salt—polymer interactions.

In most of the studies including those discussed above, the polymer matrices used to form the composites are standard polymer electrolytes with lithium salts "freely" dissolved. Thus, the matrix has low Li<sup>+</sup> transference numbers. In contrast, Li<sup>+</sup>conducting ceramics are typically single-ion conductors with a Li<sup>+</sup> transference number very close to 1. This transference number mismatch causes polarization at the polymer—ceramic interface.<sup>33</sup> To date, composite electrolytes using SIC polymers as the host have largely been unexplored.<sup>14,34,35</sup>

In this work, we synthesized SIC polymers by cross-linking poly(ethylene glycol) dimethacrylate (PEGDMA) with ioncontaining monomers including 4-styrenesulfonyl-(trifluoromethylsulfonyl)imide (STFSI) and 4-vinylbenzenesulfonate (SS). A doped LATP type ceramic, LICGC, and an amorphous ceramic, lithium lanthanum titanium oxide (LLTO), were used as the fillers to form composites. We report the effects of these Li<sup>+</sup>-conducting ceramic particles on the physical, thermal, mechanical, ion transport, and electrochemical properties of the SIC composites. These properties were also compared with the non-single-ion-conducting counterpart using a polymer host with the same PEGDMA backbone and freely dissolved lithium salt (lithium bis-(trifluoromethanesulfonyl)imide, LiTFSI). The comparison sheds light on how to optimize the polymer host chemistry to form composite electrolytes toward a stable lithium metal anode. This work is part of a series of systematic studies on the fabrication, ion transport, and interfacial interactions in polymer-ceramic composite electrolytes. 20,30,31,36

#### 2. EXPERIMENTAL SECTION

2.1. Chemicals and Materials. Poly(ethylene glycol) dimethacrylate (PEGDMA, approximate molecular weight 1000 g/mol) was purchased from Polysciences and used without further purification. Sodium 4-vinylbenzenesulfonate (NaSS), tetraethylene glycol dimethyl ether (TEGDME), acetonitrile, and 2,2'-azobis(2-methylpropionitrile) (AIBN) were purchased from Sigma Aldrich. TEGDME was dried on molecular sieves prior to use. AIBN was recrystallized from methanol before use. Dimethyl sulfoxide (DMSO) was purchased from Alfa Aesar. Lithium bistrifluoromethanesulfonimide (LiTFSI) was purchased from 3M and dried under vacuum at 150 °C for at least 24 h prior to use. The potassium 4-styrenesulfonyl-(trifluoromethylsulfonyl)imide (KSTFSI) monomer was synthesized as described in previous reports. 9,37 Lithium-ion-conducting glass ceramic powder (LICGC) was purchased from Ohara Corporation. It is a doped LATP ceramic with the general composition of Li<sub>2</sub>O-Al<sub>2</sub>O<sub>3</sub>-SiO<sub>2</sub>-P<sub>2</sub>O<sub>5</sub>-TiO<sub>2</sub>-GeO<sub>2</sub>. It is air- and water-stable. The average particle size of the powder used was 1  $\mu$ m. Amorphous LLTO powder was obtained via an all-alkoxide route<sup>38</sup> as described in previous works.<sup>39-41</sup> Lithium isopropoxide (10 mol % extra added to compensate for lithium loss) and titanium isopropoxide were added into lanthanum 2-methoxyethoxide based on the stoichiometric ratio of  $Li_{0.35}La_{0.55}TiO_3$  (LLTO). The mixture was refluxed in a glovebox for 2 h, and subsequently, 10 mol % water was slowly dropped into the mixed solution to accelerate the gel formation. With the mixed solution converted to gel, it was first dried in an oven at 80 °C and then calcined in a furnace at 120 and 450 °C to fully remove the organic solvent. The target LLTO powder was obtained after grinding for 30 min to achieve uniform particle size.

2.2. Synthesis and Fabrication of Polymer and Composite **Electrolyte Films.** SIC polymer films were prepared by combining PEGDMA and the anion monomer (NaSS or KSTFSI) to the desired [EO]:[Charge] molar ratio of 45 in DMSO (1.2 mL of solvent/g monomer). 1 wt % AIBN was added to the solution as the thermal initiator. The solution was then cast and sandwiched between two glass plates with glass slides used to standardize film thickness (110 to 150  $\mu$ m). The resulting film was allowed to cross-link for 1 h at 75 °C. After cross-linking was completed, the Na+- or K+-containing polymer electrolyte films were exchanged to Li<sup>+</sup> via an aqueous ion exchange process as described in previous works.<sup>9,42</sup> Briefly, the films were soaked in LiBr solution for 48 h with the solution changed out two times a day. This step exchanges Na+ or K+ to Li+ and washes out the residual DMSO solvent in the films. Then the films were washed with deionized water for 24 h with the water exchanged out twice. The films were dried in ambient conditions overnight and then were transferred into an argon-filled glovebox where they were dried in a vacuum furnace inside the glovebox at 80 °C overnight. The completion of Li+ exchange was confirmed via inductively coupled plasma-optical emission spectroscopy (ICP-OES). The Na<sup>+</sup> and K<sup>+</sup> remaining in the films after ion exchange were deemed negligible via

To compare results with SIC polymers and composites, PEGDMA was also cross-linked with the presence of free LiTFSI salt using the same setup and procedure as described above. Since Li<sup>+</sup> exchange is not necessary after cross-linking, acetonitrile was used instead of DMSO to avoid the washing steps. The film drying procedure was the same as described above.

Ceramic-containing composite electrolytes were prepared by first mixing calculated weights of LICGC or LLTO particles into the monomer solution. The mixture was ball-milled for 30 min. The cross-linking, ion exchange, washing, and drying procedure for SIC composite electrolytes were the same as those for the SIC polymer electrolyte. Similarly, the cross-linking and drying procedure of free-salt-containing polymer and composite electrolytes were kept the same

After thorough drying of the polymer and composite electrolyte films, the films were ready for use in the dry state. In order to improve the conductivity of the films to enable cycling, part of the dried films was cut out and plasticized with TEGDME. The SIC polymer and

composite films were immersed in TEGDME for 1 h. For the non-SIC polymer and composite films, 20  $\mu$ L of TEGDME was added onto the films to allow plasticization. This amount ensures a saturated amount of TEGDME to be absorbed into the films while preventing LiTFSI salt from leaching out of the films. Figure S1 compares the conductivity of plasticized films with and without salt leaching. The plasticized films were dabbed dry with Kimwipe before measurements to avoid flooding of TEGDME.

**2.3. Conductivity Measurements.** Conductivity measurements were taken using a Biologic SP-300 from 7 MHz to 0.1 Hz with an AC voltage of 100 mV. Polymer and composite electrolyte films were punched into 1/2 in. disks and sandwiched between two polished stainless steel rods. The sample was sealed with two layers of heat shrink tubing. The resultant Nyquist plots were fit using equivalent circuits, and the bulk resistance of the polymer was used to calculate the conductivity.

The molar conductivity of the polymer films was calculated by dividing the resultant ionic conductivity by the concentration in mol/cm³. The dry mass of the film was used to calculate the moles of lithium in the film, based on the Li<sup>+</sup> concentration determined through ICP-OES. Then the film was swelled in TEGDME, and the swelled dimensions were used to calculate the volume of the film.

**2.4. Cycling Measurements.** Cycling measurements of polymer and composite electrolytes were taken in a symmetric coin cell configuration. All samples were plasticized in TEGDME prior to measurement using the procedure described above. Lithium electrodes were cleaned with a brush to remove the oxide layer and then rolled out using a clean polypropylene bag to smooth the surface. CR2032 coin cells were assembled in an argon-filled glovebox.

Cycling measurements were carried out using a Biologic potentiostat in a temperature chamber set to 70 °C. A current of  $50~\mu\text{A/cm}^2$  was applied for 30 min and then reversed. Impedance measurements were taken every 10 cycles with an AC voltage of 10 mV and a frequency range between 7 MHz and 0.1 Hz.

**2.5. Transference Number Measurements.** Transference number measurements were taken using the Bruce and Vincent method with a Biologic SP-300. The symmetric cells were cycled at  $0.01 \text{ mA/cm}^2$  for 4 h for each charge/discharge segment to stabilize the interface between the polymer and the lithium metal. After cycling, the impedance was measured, and then the cell was polarized for 10 h at 10 mV, after which the impedance was measured again. The impedance of the cells was taken between 7 MHz and 0.1 Hz with an amplitude of 10 mV. The steady-state transference number  $(t_{\rm SS}^+)$  was then calculated using eq 1, where  $R_0$  is the resistance measured prior to applying the potential  $(\Delta V)$ ,  $I_0$  is the initial current measured at the beginning of the polarization, and  $I_{\rm SS}$  and  $R_{\rm SS}$  are the steady-state current and resistance measured after polarization, respectively.

$$t_{\rm SS}^{+} = \frac{I_{\rm SS}}{I_0} \left( \frac{\Delta V - I_0 R_0}{\Delta V - I_{\rm SS} R_{\rm SS}} \right) \tag{1}$$

- **2.6. Raman Spectroscopy.** Raman spectra were taken using a confocal Raman microscope (WITec, Alpha 300) with a 20× objective lens and a 532 nm wavelength laser. The grating was set to 1800 grooves/mm, and the local laser power was measured to be around 500  $\mu$ W using a digital meter (Thorlabs, PW100D). Total sample exposure time was 90 s.
- **2.7. Differential Scanning Calorimetry (DSC).** Calorimetry measurements were taken using a TA Instruments Q100 DSC. The samples were loaded into aluminum pans and crimped in an argonfilled glovebox. The samples contained at least 5 mg of polymeric material. For each measurement, the sample was equilibrated at -80 °C under a nitrogen flow of 50 mL/min. The temperature was then increased to 150 °C at a scan rate of 5 °C/min. After a 5 min hold at 150 °C, the temperature was decreased to -80 °C and increased again to 150 °C at the same scan rate. The second cycle was used to calculate the glass transition temperature ( $T_{\rm g}$ ) of the sample.
- **2.8. Physical Properties.** Dynamic mechanical analysis (DMA) measurements were performed on the plasticized films using a TA

Instruments RSA-G2 solid analyzer. A small tensile strain of 0.1-0.3% was applied at 10 Hz. Measurements were taken between 20 and 90 °C under nitrogen flow. The densities of the polymers and composites were measured in the dry state using a gas pycnometer (Micromeritics AccuPyc II 1340) under helium gas at 20 °C. Samples were sealed inside the glovebox to minimize air exposure during the transfer to the instrument.

**2.9. Scanning Electron Microscopy/Energy-Dispersive X-ray Spectroscopy (SEM/EDS).** SEM/EDS measurements were taken using a TM3030Plus Tabletop Microscope from Hitachi. The accelerating voltage used was 15 kV, and the images were taken using both secondary electrons (SE) and backscattering electrons (BSE).

#### 3. RESULTS AND DISCUSSION

**3.1. Film Preparation and Physical Properties.** We prepared SIC polymers by cross-linking the ion-transporting component, PEGDMA, with ion-containing monomers, STFSI and SS. The chemical structures of these components are shown in Figure 1a. A previous study has shown that the highly

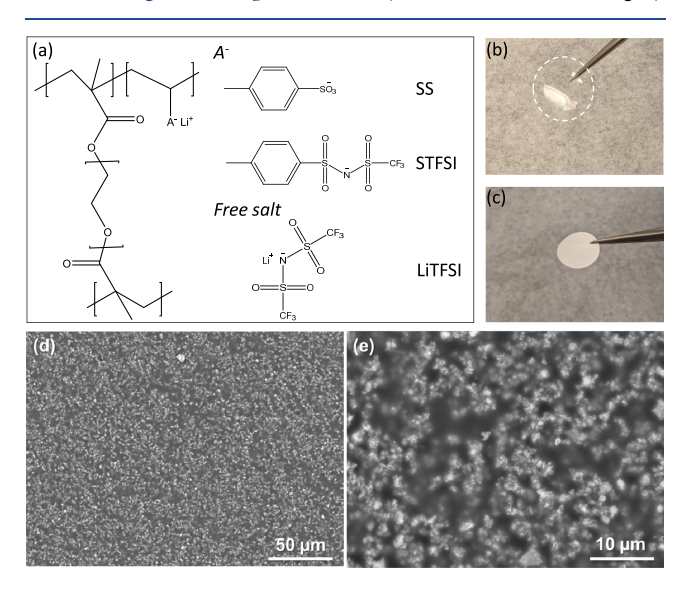


**Figure 1.** (a) Chemical structures of polymer electrolytes synthesized in this work. (b) Photograph of the cross-linked PEGDMA-co-STFSI film without ceramic. (c) Photograph of composite PEGDMA-co-STFSI with 50 wt % LICGC. (d,e) SEM images of PEGDMA-co-STFSI with 50 wt % LICGC: (d) 1000× magnification; (e) 5000× magnification.

dissociable STFSI anion has significantly increased ionic conductivities compared to the hard SS anion. This is related to the electron-withdrawing groups on the STFSI anion along with the increased flexibility of the anion itself. As a parallel comparison, we also prepared non-SIC polymer electrolytes by cross-linking PEGDMA with the presence of free LiTFSI salt. These samples are coded and listed in Table 1. The details of the synthesis and film fabrication are described in the Experimental Section. The [EO]:[Charge] ratio was kept constant at 45 as previous work found this ratio to be highly conductive.

The model ceramic we chose to use in this work is a Li<sup>+</sup>-conducting LATP type ceramic, LICGC. This ceramic electrolyte has high room-temperature ionic conductivity (1  $\times$  10<sup>-4</sup> S/cm), and it is stable in air and water. The ceramic was incorporated into the electrolyte films before the cross-linking step (see the Experimental Section). The addition of 50 wt % ceramic into the polymer electrolyte resulted in an

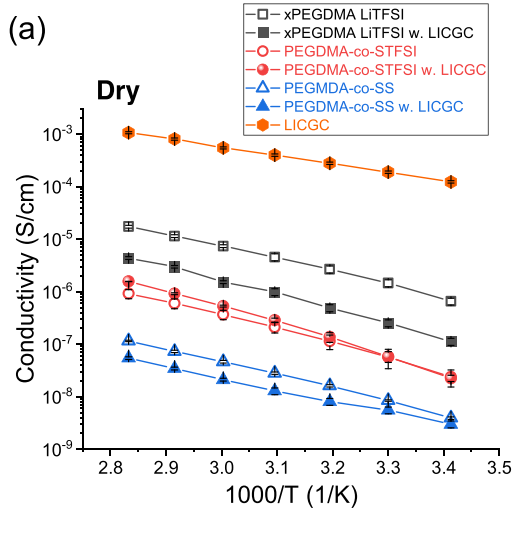
Table 1. Measured Densities of Polymers with and without a Tethered Anion and with and without LICGC Particles

sample	density (g/cm³)	% increase from xPEGDMA	vol % of LICGC
xPEGDMA	$1.333 \pm 0.069$	N/A	N/A
xPEGDMA with LiTFSI	$1.422 \pm 0.004$	6.6%	N/A
xPEGDMA with LiTFSI and LICGC	$2.104 \pm 0.002$	57.8%	34.5%
PEGDMA-co-STFSI	$1.474 \pm 0.002$	10.6%	N/A
PEGDMA-co-STFSI with LICGC	$2.223 \pm 0.006$	66.7%	36.4%

opaque and flexible film with significantly enhanced handle-ability and decreased brittleness (Figure 1c). Without the ceramic, the polymer films are prone to tear and sticking to themselves (Figure 1b). In other words, the processability of the composite is enhanced compared to that of the neat polymer electrolyte. The storage moduli of TEGMDE-plasticized PEGDMA-co-STFSI polymers with and without the LICGC particles were obtained by performing DMA measurements (results shown in Figure S2). The composite polymer electrolyte (CPE) shows an increased modulus compared to the pristine polymer electrolyte. SEM images of the composite electrolytes were taken to confirm that the ceramic particles were well dispersed throughout the polymer matrix, shown in Figure 1d,e. Figure S3 shows the corresponding EDS mapping of Figure 1e.

The densities of polymer electrolytes and composite electrolytes with 50 wt % ceramic were measured using a gas pycnometer. As shown in Table 1, the addition of 50 wt % ceramic particles significantly increased the density of the composites, by approximately 50% compared to the polymer electrolyte (PE) with either the free salt or covalently bound salt. The increase in density from the cross-linked PEGDMA polymer matrix is slightly greater for the PE with the bound anion (STFSI) than with the free anion (TFSI), likely related to the disruption of the PEGDMA matrix to adjust for the covalently bound anion and greater mass of the anion. Using the density of LICGC ceramic (3.05 g/cm<sup>3</sup>)<sup>20</sup> and assuming that the primary particles are non-porous and incompressible, we calculated the volume fractions of the ceramic in xPEGDMA with LiTFSI and PEGDMA-co-STFSI to be 34.5 and 36.4%, respectively.

3.2. Ionic Conductivity. Ionic conductivity measurements of the dry polymer and composite polymer films were taken between 20 and 80 °C, shown in Figure 2a. The error range was calculated based on repeats of 2-3 samples. In our previous studies of composite polymer electrolytes, the addition of ceramic particles to the polymer matrix lowered the conductivity compared to the pristine non-SIC polymer electrolytes containing LiTFSI and lithium trifluoromethanesulfonate (LiTf) salts. 20,31 We see this again in the polymer matrices with the free LiTFSI salt and with the hard covalently bound SS anion. However, evident from Figure 2a, the addition of the ceramic particles does not lower the conductivity in the case of the highly dissociable STFSI anion. The SIC polymers and composites have decreased conductivity compared to the LiTFSI-containing polymer and composite electrolyte, which is expected as both the cation and anion are mobile in the latter. The conductivity of the dense LICGC plate is also displayed in Figure 2a, which is 3-4 orders of magnitude higher than the SIC polymers.



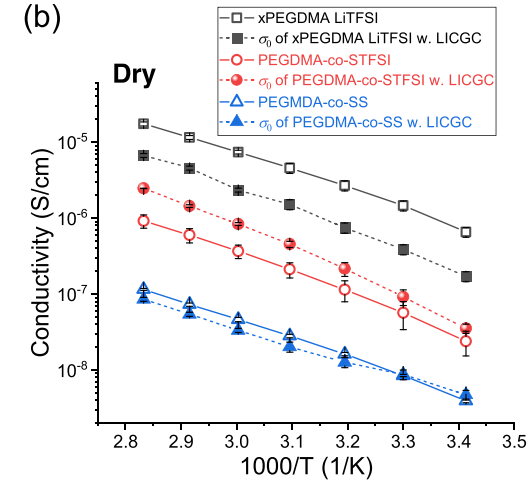


**Figure 2.** (a) Conductivity of polymer and composite electrolytes as a function of inverse temperature in the dry state and (b) intrinsic conductivity of the polymer phase in the composite electrolytes as a function of inverse temperature, compared to the measured conductivity of the polymer electrolytes without ceramic.

The ionic conductivity of a mixed material may be calculated using the following first-order equation. This first-order approximation ignores any tortuosity within the polymer network.

$$\sigma_{\text{CPE}} = \phi_{\text{polymer}} \sigma_{0,\text{polymer}} + \phi_{\text{ceramic}} \sigma_{\text{ceramic}}$$
(2)

In eq 2,  $\sigma_{\rm CPE}$  is the experimentally measured ionic conductivity of the composites and  $\phi_{
m polymer}$  and  $\phi_{
m ceramic}$  are the volume fractions of the polymer and the ceramic, respectively.  $\phi_{\text{ceramic}}$  was calculated from gas pycnometry results, as shown in Table 1.  $\sigma_{0,\mathrm{polymer}}$  and  $\sigma_{\mathrm{ceramic}}$  are the intrinsic ionic conductivities of the polymer and the ceramic, respectively. If the ceramic particles participated in ion conduction in the composites, according to eq 2, the conductivity of the composites would be between  $5 \times 10^{-5}$ and  $4 \times 10^{-4}$  S/cm in the measured temperature range. The actual measured conductivity of the composites regardless of the polymer matrix chemistry was at least 1 order of magnitude smaller than that. Therefore, our results indicate that the ceramic particles most likely did not actively participate in ion conduction in these composites. This assumption is further corroborated by our past works, where we used combined EIS

and quasi-elastic neutron scattering and discovered that there was a large interfacial resistance between the polymer and ceramic phases that did not allow for facile ion transport between the ceramic and the polymer. <sup>30,31</sup>

We then assume that the second term in eq 2 can be eliminated as the ceramic's effective conductivity is zero.<sup>31</sup> The ionic conductivity may be approximated using the first term of the equation, shown in eq 3.

$$\sigma_{\text{CPE}} = \phi_{\text{polymer}} \sigma_{0,\text{polymer}} \tag{3}$$

Using  $\phi_{\text{polymer}} = 1 - \phi_{\text{ceramic}}$ , we can estimate the intrinsic ionic conductivity of the polymer phase in the composite. In Figure 2b, we plot  $\sigma_{0,\text{polymer}}$  in the three composites and compare them with their respective neat polymer electrolyte. Evidently,  $\sigma_{0,\text{polymer}}$  in the non-SIC polymer containing the free LiTFSI was only ~30% of the conductivity of the neat polymer. This is consistent with our previous studies.  $^{31,32}$ 

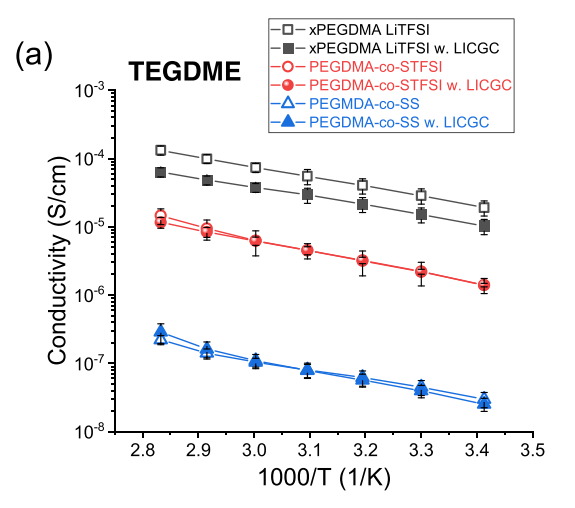
In contrast,  $\sigma_{0,polymer}$ s in SIC-polymer-based composites show a different trend.  $\sigma_{0,polymer}$  in the SS-containing SIC composite is on average 85% of the conductivity of the neat polymer, which is lower than the neat polymer, but an increase compared to the non-SIC case. Furthermore,  $\sigma_{0,polymer}$  of the STFSI-containing SIC composite is on average 210% of the conductivity of the neat PEGDMA-co-STFSI. This systematic comparison revealed that the addition of high loadings of LICGC ceramic can enhance the ionic conductivity of the SIC polymer containing highly dissociable anions. The underlying mechanism of this intrinsic conductivity enhancement will be discussed later.

When the polymers and the composites were plasticized with TEGDME, as shown in Figure 3, the ionic conductivity increased compared to that of the dry state. This is likely due to a combination of mechanisms, such as an increase of Li<sup>+</sup> dissociation in the polymer, increased segmental dynamics, and change of the ion transport mechanism from hopping to vehicular transport. Interestingly, the conductivity of the SIC systems was the same for the composite and the pristine polymer electrolyte. When comparing the molar conductivities of the electrolytes, the LICGC-containing composite with the SS anion had a slightly increased conductivity (average 9%) compared to the neat polymer. The molar conductivity of the composite with the STFSI anion had a further increase, 40% on average, compared to that of the corresponding polymer. This indicates that the solvent must help dissociate the cations and the primary transport mechanism is vehicular for both cases. The conductivities at 70 °C in the dry and plasticized states and calculated activation energies of the polymers and the composites are tabulated in Table 2.

The glass transition temperatures  $(T_{\rm g})$  of the polymers and composites in the dry state, determined from DSC measurements, are also tabulated in Table 2. The DSC thermograms are shown in Figure S4.  $T_{\rm g}$  did not significantly change with the addition of the ceramic particles. The  $T_{\rm g}$  of the TEGDME-plasticized samples could not be measured as the crystallization/melting dynamics of the TEGDME (-45 °C) masked the region in which the  $T_{\rm g}$  would be observed.

3.3. Ceramic Loading and Ceramic Material. The

**3.3. Ceramic Loading and Ceramic Material.** The ceramic loading was varied for the PEGDMA-co-STFSI matrix to determine if the conductivity could be further improved, shown in Figure 4a. We observed an increase in the ionic conductivity for the composites containing 30 and 50 wt % LICGC, corresponding to 16 and 36 vol %, respectively. At 70 wt % or 53 vol %, the conductivity of the composite decreased



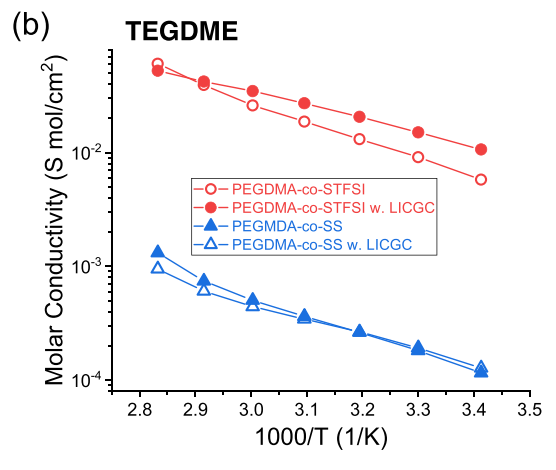


**Figure 3.** (a) Conductivities of polymers and composites plasticized with TEGDME. (b) Molar conductivity of single-ion-conducting polymers with and without LICGC particles.

compared to that of the neat PEGDMA-co-STFSI. In Figure 4b, we plot the intrinsic conductivity of the polymer phase,  $\sigma_0$ , in each composite using eq 3 and compare it with the neat polymer. Evident from Figure 4b,  $\sigma_0$  increased in the entire investigated ceramic loading range, further confirming the positive effects of LICGC ceramic on the ion transport of the STFSI-containing SIC polymer. The change in  $\sigma_0$  as a function of ceramic loading was not monotonic: as ceramic loading increases,  $\sigma_0$  first increased as more interfacial interactions with the ceramic are favorable for ion transport in the polymer matrix. As the ceramic loading further increased to greater than 50 vol %, the polymer phase may have become too tortuous and lost a continuous path for ion conduction, and  $\sigma_0$  thus decreased

To determine if we would see the same effect with other Li<sup>+</sup>-conducting ceramics, we also made electrolytes with amorphous lithium lanthanum titanate (LLTO). Amorphous LLTO was used instead of lithium lanthanum zirconium oxide (LLZO) due to its increased stability in ambient conditions. Compared to crystalline LLTO, amorphous LLTO presents two main advantages. First, due to its open disordered and isotropic structure, amorphous LLTO has good ionic conductivity and minimized grain boundary effects. Second, the electrochemically stable voltage window is high (up to 12 V) in direct contact with lithium metal. Two polymer matrices were used for the incorporation of LLTO, the non-SIC

Table 2. Glass Transition Temperatures,  $T_{\rm g}$ , Conductivities at 70 °C, and Activation Energies for the Polymer Systems Studied Dry and in TEGDME

polymer	$T_{\rm g}$ (K)	$\sigma$ (dry) at 70 °C (S/cm)	$E_{\rm a}$ (dry) (eV)	$\sigma$ (TEGDME) at 70 °C (S/cm)	$E_{\rm a}$ (TEGDME) (eV)
xPEGDMA LiTFSI	227.6	$1.2 \times 10^{-5}$	0.48	$9.9 \times 10^{-5}$	0.28
xPEGDMA LiTFSI 50 wt % LICGC	227.1	$3.0 \times 10^{-6}$	0.55	$4.8 \times 10^{-5}$	0.27
PEGDMA-co-LiSTFSI	233.3	$9.2 \times 10^{-7}$	0.54	$9.5 \times 10^{-6}$	0.34
PEGDMA-co-LiSTFSI 50 wt % LICGC	235.0	$1.6 \times 10^{-6}$	0.63	$9.0 \times 10^{-6}$	0.31
PEGDMA-co-LiSS	225.6	$9.6 \times 10^{-8}$	0.50	$3.6 \times 10^{-7}$	0.28
PEGDMA-co-LiSS 50 wt % LICGC	226.7	$3.5 \times 10^{-8}$	0.42	$2.3 \times 10^{-7}$	0.34

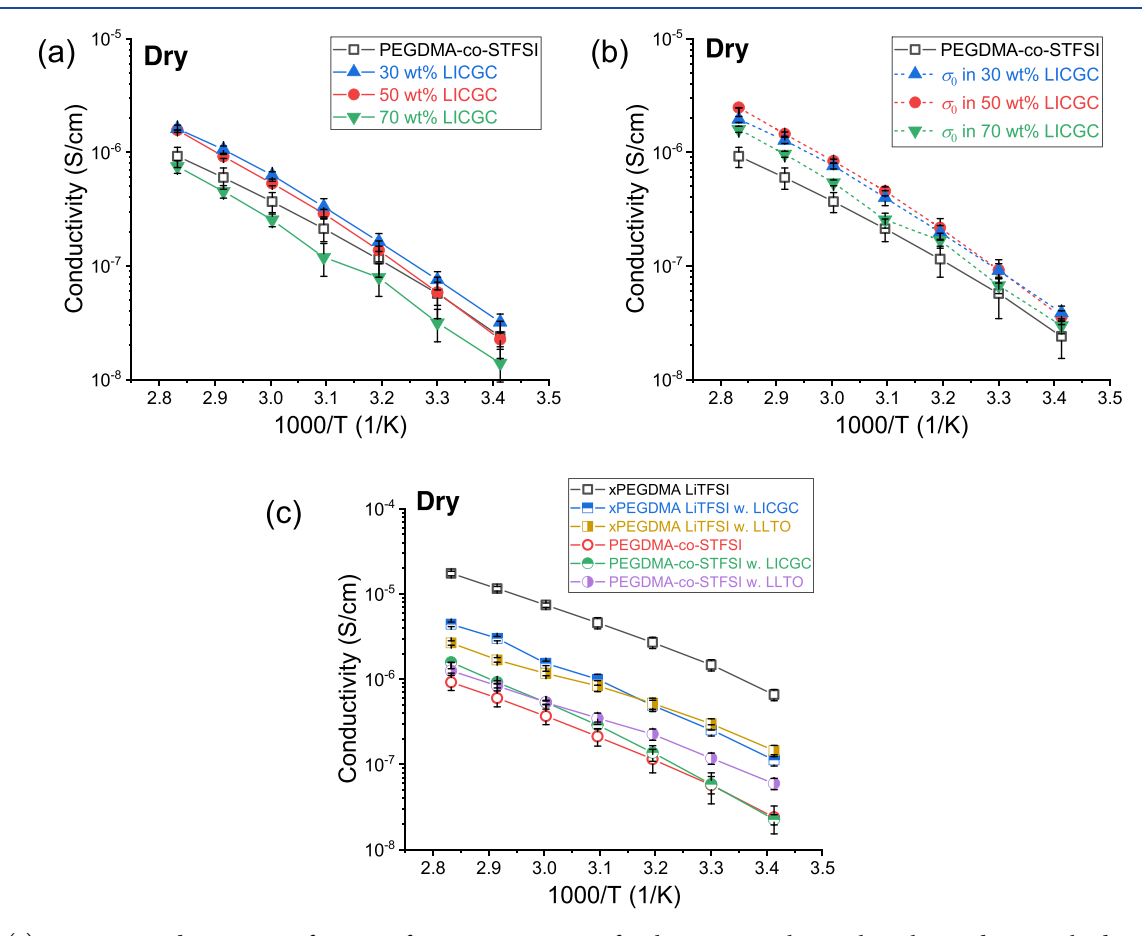


**Figure 4.** (a) Dry-state conductivity as a function of inverse temperature for the pristine polymer electrolyte and various loadings of LICGC ceramic particles. (b) Intrinsic conductivity of the polymer phase in the composite electrolytes as a function of inverse temperature, at various LICGC loadings. (c) Dry-state conductivity as a function of 1000/T for the pristine polymer electrolytes with LICGC particles and with LLTO particles.

polymer electrolyte *x*PEGDMA with LiTFSI, and the SIC polymer PEGDMA-*co*-STFSI. The LLTO loading in both composites was kept at 50 wt %. The results are shown in Figure 4c. Similar trends to LICGC were observed: the addition of LLTO decreased the ionic conductivity of the composite with the non-SIC polymer matrix, whereas the ionic conductivity increased for the SIC polymer matrix. Comparing LLTO with LICGC, the LLTO-containing composite electrolytes have lower activation energies in both polymer matrices, which led to a higher room-temperature conductivity. This comparison suggests that the positive effect of the ceramic on the conductivity of the SIC polymer is not limited to LATP type ceramic.

**3.4.** Symmetric Cell Cycling and Transference Number. To gauge the ability of the polymer and composite polymer electrolytes to plate and strip lithium, the LiTFSI- and the STFSI-containing polymers and composites were cycled at

 $50~\mu A/cm^2$  at  $70~^{\circ}C$ . For this study, we used composites containing 50~ wt % LICGC (before plasticization). Each polymer/composite was plasticized with TEGDME to decrease the resistance across the cell. Due to the single-ion conductor's lower conductivity, the overpotential was increased compared to that of the free salt case, as shown in Figure 5.

Impedance measurements were taken every 20 cycles between 1 MHz and 0.1 Hz with an amplitude of 10 mV. Figure S5 shows the impedance change from the cycling of the STFSI-containing polymers. Although the composite polymer electrolytes have a greater overpotential initially, the overpotential appears to stabilize whereas the overpotential of the pristine polymer continues to increase. From the impedance spectra, the interfacial impedance increase with cycling is more significant for the pristine polymers without the added ceramic. This suggests that a passivation layer is forming at the interface while cycling. Because the increase is greater for the pristine

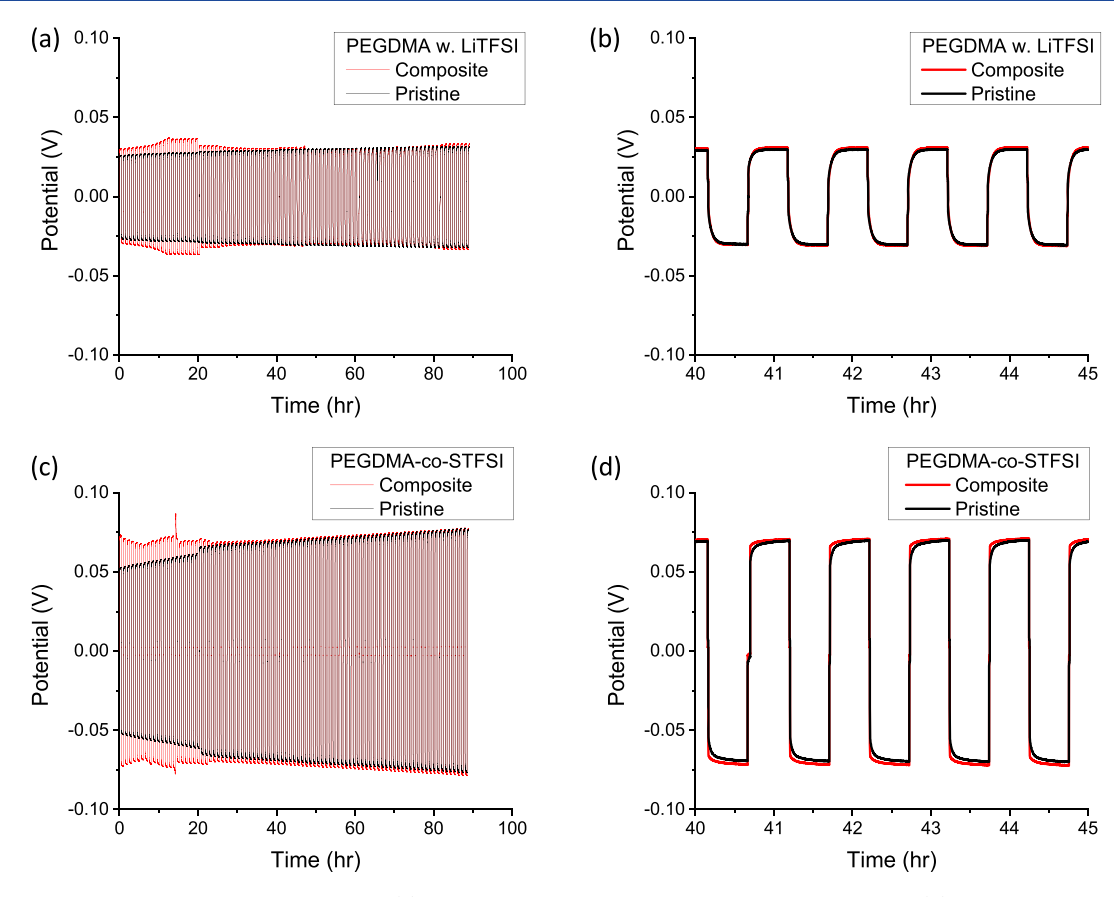


Figure 5. Symmetrical cell cycling of Li/Li cells with (a) composite and pristine xPEGDMA with LiTFSI and (b) corresponding detailed cycling from 40 to 45 h. (c) Composite and pristine PEGDMA-co-STFSI and (d) corresponding detailed cycling from 40 to 45 h.

case, the instability is likely caused by either the polymer chemistry or the TEGDME.

The measured transference numbers for LiTFSI- and STFSIcontaining polymers and composites are tabulated in Table 3,

Table 3. Tabulated  $t^+$  Values of the Polymer and Composite Electrolytes Swelled in TEGDME

polymer (plasticized with TEGDME)	measured $t^+$
PEGDMA-co-STFSI	0.90
PEGDMA-co-STFSI with LICGC	0.88
xPEGDMA with LiTFSI	0.26
xPEGDMA with LiTFSI and LICGC	0.58

and the impedance spectra and polarization are shown in Figures S6 and S7. The non-unity transference number measured for the single-ion conductors is likely due to impurities present in the electrolyte or solvent. The transference number doubles with the addition of the LICGC particles for the polymer containing free LiTFSI. The reason for the transference number increase will be explained shortly.

**3.5. Ion Association.** In the last part of the study, we discuss the effect of LICGC ceramic on the ion association of the LiTFSI-containing non-SIC composite and the STFSI-containing SIC composite. In order to understand this effect, we quantified the percentage of coordinated TFSI/STFSI anions via Raman spectroscopy, shown in Figure 6. The CF<sub>3</sub> peak around 745 cm<sup>-1</sup>, referred to as the "TFSI breathing stretch", can be used to approximate the dissociated/associated TFSI. <sup>9,11,46–48</sup>

In the case of the pristine polymer electrolyte with LiTFSI, shown in Figure 6a, a single peak is observed at 742 cm<sup>-1</sup>, suggesting that the TFSI anion is in a completely dissociated state when dissolved in xPEGDMA. In contrast, with the addition of the LICGC particles, a shoulder forms at an increased wavenumber, around 750 cm<sup>-1</sup>, suggesting that a percentage of the TFSI anions are associated in the composite (Figure 6b). Through peak fitting and integration, we determined that in the xPEGDMA + LiTFSI + 50 wt % LICGC composite, 58% of the TFSI anions are associated.

In previous works, we conducted quasi-elastic neutron scattering (QENS) and solid-state nuclear magnetic resonance (NMR) experiments to investigate the salt-polymer-ceramic three-body interactions in LICGC-containing non-SIC composite electrolytes. 31,32 We discovered that the segmental mobility of the polymer (poly(ethylene oxide) in these studies) as well as the cation (Li<sup>+</sup>) and anion mobilities all decreased with the addition of the ceramic. This was attributed to the strong affinity between the lithium salt and the ceramic surface, leading to reduced polymer segmental mobility and ion mobilities at the polymer-ceramic interface. Moreover, the ceramic surface primarily interacted with the anions dissolved in the polymer. The Raman results presented in Figure 6a,b are consistent with our previous findings as the data suggests that 58% of the TFSI anions are coordinated with the LICGC ceramic. The Raman results also explain why a 100% increase in the Li<sup>+</sup> transference number was achieved with the incorporation of LICGC ceramic into xPEGDMA + LiTFSI. The decrease in conductivity in the composite compared to the neat polymer electrolyte is primarily the result of decreased

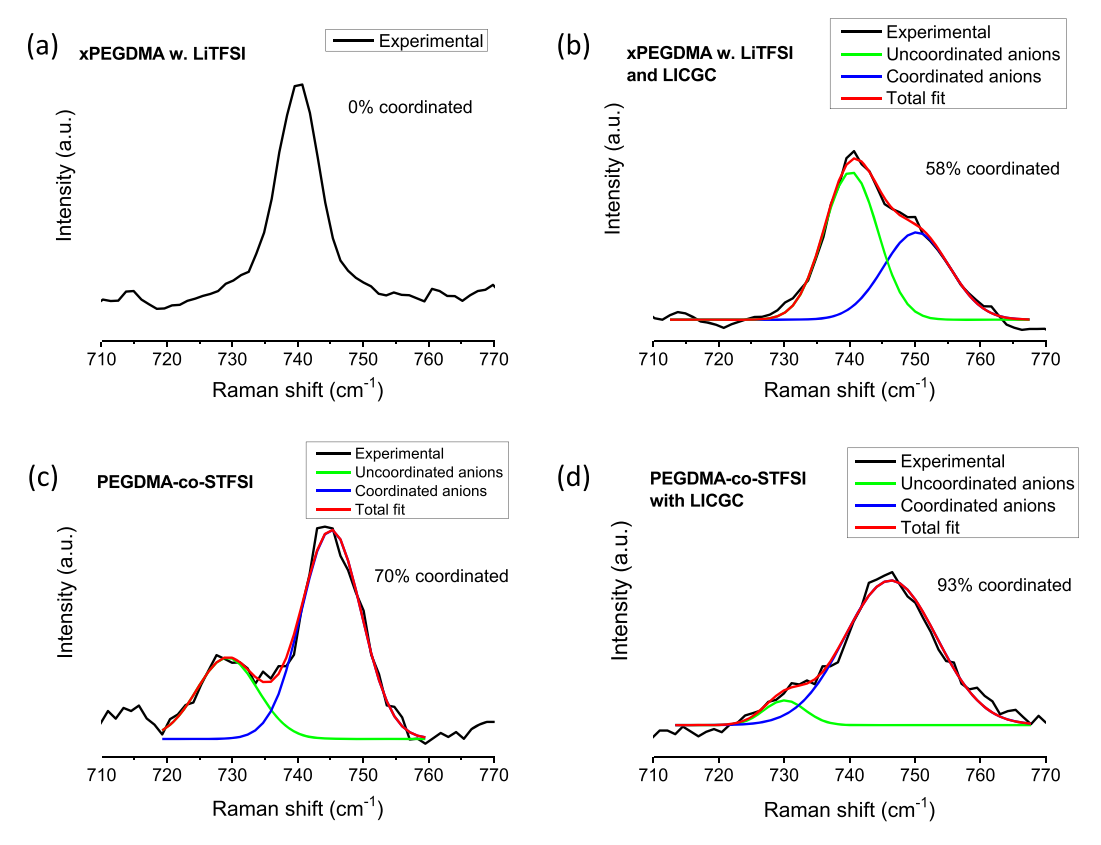


Figure 6. Fitting of the Raman spectra of the TFSI breathing stretch for dry-state (a) xPEGDMA with LiTFSI, (b) xPEGDMA with LiTFSI and LICGC ceramic particles, (c) PEGDMA-co-STFSI, and (d) PEGDMA-co-STFSI with LICGC ceramic particles.

anion conductivity, whereas the Li<sup>+</sup> conductivity was largely unaffected, as Figure S8 shows.

In the case of the STFSI-containing SIC polymer without ceramic particles, shown in Figure 6c, approximately 70% of the STFSI anions are associated, indicating that in the pristine polymer, the majority of STFSI anions and the lithium cations are tied together. For a single-ion conductor, the Li+ transference number approaches unity as the anion is covalently bound to the polymer and is subsequently immobilized. Therefore, the measured conductivity is proportional to the number of lithium ions that are not coordinated with the anion. The cations that are coordinated with the anion will have a lower degree of ionic mobility and will contribute less to the measured ionic conductivity. 48 With the addition of the ceramic particles, the ratio of coordinated STFSI anions increased to approximately 93%, shown in Figure 6d. Considering the increase in conductivity observed in the SIC composite in the dry state, this result suggested that the STFSI anion is able to coordinate with the LICGC particles. The ability of the STFSI anion to coordinate with the LICGC particles in turn helps to increase the degree of Li<sup>+</sup> dissociation, effectively increasing the number of mobile charge carriers in the polymer, thereby increasing the conductivity. The complete Raman spectra are shown in Figure S9.

We now make a comparison of the effect of ceramic addition to the two SIC polymer matrices. In the dry case, in both SIC composites, the ceramic competes with the counter ion (Li<sup>+</sup>) in coordinating with the anions. The SS anion is less flexible, and thus, Li<sup>+</sup> is less dissociable. Recall that the SS-containing SIC composite exhibited a decrease in conductivity with the addition of the ceramic particles, but the extent of the decrease was less than that of the non-SIC case. This suggests that the

SS anions do not interact strongly with the ceramic particles, and hence, most Li<sup>+</sup> counter ions remain bound to SS<sup>-</sup>. In contrast, the STFSI anion is highly flexible and Li<sup>+</sup> is easier to dissociate than the SS case. Therefore, in the STFSI-containing SIC composite, the ceramic is able to coordinate with STFSI- and free up the Li<sup>+</sup>.

When the plasticizer TEGDME was added to the composite, the activation energy decreased to about half (Table 2). We deduced that TEGDME helps dissociate the Li<sup>+</sup> and the primary transport mechanism is vehicular. With the addition of LICGC, the overall conductivity remained the same compared to the neat SIC polymers, while Li<sup>+</sup> molar conductivity increased in both the SS- and the STFSI-containing composites. This suggests that with the help of TEGDME, the ceramic is able to coordinate with both the flexible and nonflexible anions and free up more Li<sup>+</sup>. From the above discussion, when considering design strategies for SIC composites, using a more flexible anion in the polymer chemistry or adding a cation dissociating agent (such as TEGDME plasticizer) is beneficial.

Last, we comment that with or without the TEGDME plasticizer, our data do not support facile ion transport across the polymer—ceramic interface; i.e., we do not have evidence indicating that the ceramics are actively contributing to ion conduction in SIC composites. Although the Li<sup>+</sup> transfer activation barriers are greatly reduced with the presence of TEGDME, additional factors such as ceramic particle surface composition may play a role in hindering the ion transport between the two materials.

#### 4. CONCLUSIONS

In this work, we investigated the effects of Li+-conducting ceramic particles, LICGC and LLTO, on the physical, thermal, mechanical, ion transport, and electrochemical properties of single-ion-conducting composites in which the anions are covalently bound to the polymer chains. We discovered that in the dry state, with the addition of ceramics, the intrinsic ionic conductivity of the SIC polymer increased. This is true even at high loadings of ceramic (>50 vol %). Raman spectroscopy revealed that STFSI anions in the SIC polymer can coordinate with the ceramic. This coordination led to increased Li+ dissociation in single-ion conductors, which is the root cause of the conductivity enhancement observed. In contrast, the addition of LICGC into the non-SIC polymer electrolyte caused a significant decrease in the intrinsic ionic conductivity of the polymer phase, an observation consistent with our previous reports, although the decrease in conductivity is offset by an increase in the Li+ transference number.

Lithium symmetrical cell cycling with the SIC and non-SIC polymers and composites was evaluated. The overpotential and interfacial impedance with Li showed improved stability with the presence of LICGC ceramic, compared to the pristine polymers, in both the SIC and non-SIC systems.

Overall, our study shows that the addition of moderate loadings (50 wt %, ~35 vol %) of Li<sup>+</sup>-conducting ceramics into single-ion-conducting polymers is beneficial. They improve the conductivities of the polymers, the processability of the electrolyte films, and cyclability. Using this strategy, the ceramic size, ceramic surface chemistry, morphology, and spatial distribution of SIC composites may be optimized to maximize the positive effects of these ceramics.

# ASSOCIATED CONTENT

## Supporting Information

The Supporting Information is available free of charge at https://pubs.acs.org/doi/10.1021/acsaem.0c01358.

Details of DMA, DSC, impedance and electrochemical measurements, and full Raman spectra (PDF)

## AUTHOR INFORMATION

## **Corresponding Author**

Xi Chelsea Chen — Chemical Sciences Division, Oak Ridge National Laboratory, Oak Ridge, Tennessee 37830, United States; orcid.org/0000-0003-1188-7658; Email: chenx@ ornl.gov

# Authors

Laura C. Merrill — Department of Chemical and Biomolecular Engineering, University of Notre Dame, Notre Dame, Indiana 46556, United States; orcid.org/0000-0001-7673-4519

Yiman Zhang — Chemical Sciences Division, Oak Ridge National Laboratory, Oak Ridge, Tennessee 37830, United States; ⊚ orcid.org/0000-0002-5468-7181

**Hunter O. Ford** — Department of Chemical and Biomolecular Engineering, University of Notre Dame, Notre Dame, Indiana 46556, United States; ocid.org/0000-0002-9510-0324

Kun Lou – The Bredesen Center for Interdisciplinary Research and Graduate Education, University of Tennessee, Knoxville, Tennessee 37996, United States; ⊙ orcid.org/0000-0003-3701-9787

**Yubin Zhang** — Department of Mechanical Engineering, Worcester Polytechnic Institute, Worcester, Massachusetts 01609, United States; oorcid.org/0000-0002-8301-2108

Guang Yang — Chemical Sciences Division, Oak Ridge National Laboratory, Oak Ridge, Tennessee 37830, United States;
orcid.org/0000-0003-0583-6272

Yangyang Wang — Center for Nanophase Materials Sciences, Oak Ridge National Laboratory, Oak Ridge, Tennessee 37830, United States; © orcid.org/0000-0001-7042-9804

Yan Wang — Department of Mechanical Engineering, Worcester Polytechnic Institute, Worcester, Massachusetts 01609, United States; orcid.org/0000-0003-1060-2956

Jennifer L. Schaefer – Department of Chemical and Biomolecular Engineering, University of Notre Dame, Notre Dame, Indiana 46556, United States; orcid.org/0000-0003-4293-6328

Nancy J. Dudney – Chemical Sciences Division, Oak Ridge National Laboratory, Oak Ridge, Tennessee 37830, United States

Complete contact information is available at: https://pubs.acs.org/10.1021/acsaem.0c01358

#### **Author Contributions**

The manuscript was written through contributions of all authors. All authors have given approval to the final version of the manuscript.

#### **Notes**

The authors declare no competing financial interest.

#### ACKNOWLEDGMENTS

This research was primarily sponsored by the U.S. Department of Energy (DOE), Office of Energy Efficiency and Renewable Energy for the Vehicle Technologies Office's Advanced Battery Materials Research Program (Tien Duong, Program Manager). This research was supported in part by an appointment to the Oak Ridge National Laboratory ASTRO Program, sponsored by the U.S. Department of Energy and administered by the Oak Ridge Institute for Science and Education. DMA experiments were conducted at the Oak Ridge National Laboratory's Center for Nanophase Materials Sciences (CNMS), which is a DOE Office of Science user facility. The LLTO synthesis was supported by National Science Foundation DMR-1608398. J.L.S. gratefully acknowledges financial support from the NSF via award DMR-1706370 for the synthesis of the monomer.

# **■** REFERENCES

- (1) Crabtree, G.; Kócs, E.; Trahey, L. The Energy-Storage Frontier: Lithium-Ion Batteries and Beyond. MRS Bull. 2015, 40, 1067–1078.
- (2) Cabana; Monconduit, L.; Larcher, D.; Palacín, M. R. Beyond Intercalation-Based Li Ion Batteries: The State of the Art and Challenges of Electrode Materials Reacting Through Conversion Reactions. *Adv. Mater.* **2010**, 22, E170–E192.
- (3) Golodnitsky, D.; Strauss, E.; Peled, E.; Greenbaum, S. Review On Order and Disorder in Polymer Electrolytes. *J. Electrochem. Soc.* **2015**, *162*, A2551–A2566.
- (4) Chen, R.; Qu, W.; Guo, X.; Li, L.; Wu, F. The Pursuit of Solid-State Electrolytes for Lithium Batteries: From Comprehensive Insight To. *Mater. Horiz.* **2016**, *3*, 487–516.
- (5) Keller, M.; Varzi, A.; Passerini, S. Hybrid Electrolytes for Lithium Metal Batteries. *J. Power Sources* **2018**, *392*, 206–225.
- (6) Zhang, H.; Li, C.; Piszcz, M.; Coya, E.; Rojo, T.; Rodriguez-Martinez, L. M.; Armand, M.; Zhou, Z. Single Lithium-Ion

- Conducting Solid Polymer Electrolytes: Advances and Perspectives. *Chem. Soc. Rev.* **2017**, *46*, 797–815.
- (7) Diederichsen, K. M.; McShane, E. J.; McCloskey, B. D. Promising Routes to a High Li+ Transference Number Electrolyte for Lithium Ion Batteries. ACS Energy Lett. 2017, 2, 2563–2575.
- (8) Ma, L.; Nath, P.; Tu, Z.; Tikekar, M.; Archer, L. A. Highly Conductive, Sulfonated, UV Cross-Linked Separators for Li-S Batteries. *Chem. Mater.* **2016**, 28, 5147–5154.
- (9) Elmore, C.; Seidler, M.; Ford, H.; Merrill, L.; Upadhyay, S.; Schneider, W.; Schaefer, J. Ion Transport in Solvent-Free, Crosslinked, Single-Ion Conducting Polymer Electrolytes for Post-Lithium Ion Batteries. *Batteries* 2018, 4, 28.
- (10) Thelen, J. L.; Inceoglu, S.; Venkatesan, N. R.; Mackay, N. G.; Balsara, N. P. Relationship between Ion Dissociation, Melt Morphology, and Electrochemical Performance of Lithium and Magnesium Single-Ion Conducting Block Copolymers. *Macromolecules* **2016**, *49*, 9139–9147.
- (11) Ketkar, P. M.; Shen, K. H.; Hall, L. M.; Epps, T. H. Charging toward Improved Lithium Ion Polymer Electrolytes: Exploiting Synergistic Experimental and Computational Approaches to Facilitate Materials Design. *Mol. Syst. Des. Eng.* **2019**, *4*, 223–238.
- (12) Shin, D.-M.; Bachman, J. E.; Taylor, M. K.; Kamcev, J.; Park, J. G.; Ziebel, M. E.; Velasquez, E.; Jarenwattananon, N. N.; Sethi, G. K.; Cui, Y.; Long, J. R. A Single-Ion Conducting Borate Network Polymer as a Viable Quasi-Solid Electrolyte for Lithium Metal Batteries. *Adv. Mater.* **2020**, 32, 1905771.
- (13) Ma, Q.; Zhang, H.; Zhou, C.; Zheng, L.; Cheng, P.; Nie, J.; Feng, W.; Hu, Y. S.; Li, H.; Huang, X.; Chen, L.; Armand, M.; Zhou, Z. Single Lithium-Ion Conducting Polymer Electrolytes Based on a Super-Delocalized Polyanion. *Angew. Chem., Int. Ed.* **2016**, 55, 2521–2525.
- (14) Xu, R.; Xiao, Y.; Zhang, R.; Cheng, X.-B.; Zhao, C.-Z.; Zhang, X.-Q.; Yan, C.; Zhang, Q.; Huang, J.-Q. Dual-Phase Single-Ion Pathway Interfaces for Robust Lithium Metal in Working Batteries. *Adv. Mater.* **2019**, *31*, 1808392.
- (15) Yan, C.; Xu, R.; Xiao, Y.; Ding, J.-F.; Xu, L.; Li, B.-Q.; Huang, J.-Q. Toward Critical Electrode/Electrolyte Interfaces in Rechargeable Batteries. *Adv. Funct. Mater.* **2020**, *30*, 1909887.
- (16) Zhou, D.; Tkacheva, A.; Tang, X.; Sun, B.; Shanmukaraj, D.; Li, P.; Zhang, F.; Armand, M.; Wang, G. Stable Conversion Chemistry-Based Lithium Metal Batteries Enabled by Hierarchical Multifunctional Polymer Electrolytes with Near-Single Ion Conduction. *Angew. Chem., Int. Ed.* **2019**, *58*, 6001–6006.
- (17) Liu, J.; Pickett, P. D.; Park, B.; Upadhyay, S. P.; Orski, S. V.; Schaefer, J. L. Non Solvating, Side-Chain Polymer Electrolytes as Lithium Single-Ion Conductors: Synthesis and Ion Transport Characterization. *Polym. Chem.* **2020**, *11*, 461–471.
- (18) Amici, J.; Romanin, S.; Alidoost, M.; Versaci, D.; Francia, C.; Smeacetto, F.; Bodoardo, S. UV-Cured Methacrylate Based Polymer Composite Electrolyte for Metallic Lithium Batteries. *J. Electroanal. Chem.* **2019**, 837, 103–107.
- (19) Falco, M.; Castro, L.; Nair, J. R.; Bella, F.; Bardé, F.; Meligrana, G.; Gerbaldi, C. UV Cross-Linked Composite Polymer Electrolyte for High-Rate, Ambient Temperature Lithium Batteries. *ACS Appl. Energy Mater.* **2019**, *2*, 1600–1607.
- (20) Pandian, A. S.; Chen, X. C.; Chen, J.; Lokitz, B. S.; Ruther, R. E.; Yang, G.; Lou, K.; Nanda, J.; Delnick, F. M.; Dudney, N. J. Facile and Scalable Fabrication of Polymer Ceramic Composite Electrolyte with High Ceramic Loadings. *J. Power Sources* **2018**, *390*, 153–164.
- (21) Li, Z.; Huang, H.-M.; Zhu, J.-K.; Wu, J.-F.; Yang, H.; Wei, L.; Guo, X. Ionic Conduction in Composite Polymer Electrolytes: Case of PEO:Ga-LLZO Composites. ACS Appl. Mater. Interfaces 2018, 11, 784–791.
- (22) Manuel Stephan, A.; Nahm, K. S. Review on Composite Polymer Electrolytes for Lithium Batteries. *Polymer* **2006**, *47*, 5952–5964
- (23) Shao, Y.; Rajput, N. N.; Hu, J.; Hu, M.; Liu, T.; Wei, Z.; Gu, M.; Deng, X.; Xu, S.; Han, K. S.; Wang, J.; Nie, Z.; Li, G.; Zavadil, K. R.; Xiao, J.; Wang, C.; Henderson, W. A.; Zhang, J.-G.; Wang, Y.;

- Mueller, K. T.; Persson, K.; Liu, J. Nanocomposite Polymer Electrolyte for Rechargeable Magnesium Batteries. *Nano Energy* **2015**, *12*, 750–759.
- (24) Zhao, B.; Lu, X.; Wang, Q.; Yang, J.; Zhao, J.; Zhou, H. Enhancing the Ionic Conductivity in a Composite Polymer Electrolyte with Ceramic Nanoparticles Anchored to Charged Polymer Brushes. *Chin. Chem. Lett.* **2020**, *31*, 831–835.
- (25) Zhang, X.; Liu, T.; Zhang, S.; Huang, X.; Xu, B.; Lin, Y.; Xu, B.; Li, L.; Nan, C.-W.; Shen, Y. Synergistic Coupling between Li<sub>6.75</sub>La<sub>3</sub>Zr<sub>1.75</sub>Ta<sub>0.25</sub>O<sub>12</sub> and Poly(Vinylidene Fluoride) Induces High Ionic Conductivity, Mechanical Strength, and Thermal Stability of Solid Composite Electrolytes. *J. Am. Chem. Soc.* **2017**, *139*, 13779–13785.
- (26) Croce, F.; Persi, L.; Scrosati, B.; Serraino-Fiory, F.; Plichta, E.; Hendrickson, M. A. Role of the Ceramic Fillers in Enhancing the Transport Properties of Composite Polymer Electrolytes. *Electrochim. Acta* **2001**, *46*, 2457–2461.
- (27) Kalnaus, S.; Sabau, A. S.; Tenhaeff, W. E.; Dudney, N. J.; Daniel, C. Design of Composite Polymer Electrolytes for Li Ion Batteries Based on Mechanical Stability Criteria. *J. Power Sources* **2012**, *201*, 280–287.
- (28) Tang, W.; Tang, S.; Zhang, C.; Ma, Q.; Xiang, Q.; Yang, Y.-W.; Luo, J. Simultaneously Enhancing the Thermal Stability, Mechanical Modulus, and Electrochemical Performance of Solid Polymer Electrolytes by Incorporating 2D Sheets. *Adv. EnergyMater.* **2018**, *8*, 1800866.
- (29) Tang, W.; Tang, S.; Guan, X.; Zhang, X.; Xiang, Q.; Luo, J. High-Performance Solid Polymer Electrolytes Filled with Vertically Aligned 2D Materials. *Adv. Funct. Mater.* **2019**, 29, 1900648.
- (30) Chen, X. C.; Liu, X.; Samuthira Pandian, A.; Lou, K.; Delnick, F. M.; Dudney, N. J. Determining and Minimizing Resistance for Ion Transport at the Polymer/Ceramic Electrolyte Interface. *ACS Energy Lett.* **2019**, *4*, 1080–1085.
- (31) Chen, X. C.; Sacci, R. L.; Osti, N. C.; Tyagi, M.; Wang, Y.; Palmer, M. J.; Dudney, N. J. Study of Segmental Dynamics and Ion Transport in Polymer-Ceramic Composite Electrolytes by Quasi-Elastic Neutron Scattering. *Mol. Syst. Des. Eng.* **2019**, *4*, 379–385.
- (32) Peng, J.; Xiao, Y.; Clarkson, D. A.; Greenbaum, S. G.; Zawodzinski, T. A.; Chen, X. C. A Nuclear Magnetic Resonance Study of Cation and Anion Dynamics in Polymer Ceramic Composite Solid Electrolytes. ACS Appl. Polym. Mater. 2020, 2, 1180–1189.
- (33) Mehrotra, A.; Ross, P. N.; Srinivasan, V. Quantifying Polarization Losses in an Organic Liquid Electrolyte/Single Ion Conductor Interface. *J. Electrochem. Soc.* **2014**, *161*, 153–A1690.
- (34) Yu, Q.; Nie, Y.; Cui, Y.; Zhang, J.; Jiang, F. Single-Ion Polyelectrolyte/ Mesoporous Hollow-Silica Spheres, Composite Electrolyte Membranes for Lithium-Ion Batteries. *Electrochim. Acta* **2015**, *182*, 297–304.
- (35) Gao, J.; Shao, Q.; Chen, J. Lithiated Nafion-Garnet Ceramic Composite Electrolyte Membrane for Solid-State Lithium Metal Battery. *J. Energy Chem.* **2020**, *46*, 237–247.
- (36) Palmer, M. J.; Kalnaus, S.; Dixit, M. B.; Westover, A. S.; Hatzell, K. B.; Dudney, N. J.; Chen, X. C. A Three-Dimensional Interconnected Polymer/Ceramic Composite as a Thin Film Solid Electrolyte. *Energy Storage Mater.* **2020**, *26*, 242–249.
- (37) Meziane, R.; Bonnet, J. P.; Courty, M.; Djellab, K.; Armand, M. Single-Ion Polymer Electrolytes Based on a Delocalized Polyanion for Lithium Batteries. *Electrochim. Acta* **2011**, *57*, 14–19.
- (38) Zheng, Z.; Zhang, Y.; Song, S.; Wang, Y. Sol-Gel Processed Amorphous Inorganic Lithium Ion Electrolyte Thin Films: Sol Chemistry. *RSC Adv.* **2017**, *7*, 30160–30165.
- (39) Zhang, Y.; Zheng, Z.; Liu, X.; Chi, M.; Wang, Y. Fundamental Relationship of Microstructure and Ionic Conductivity of Amorphous LLTO as Solid Electrolyte Material. *J. Electrochem. Soc.* **2019**, *166*, A515–A520.
- (40) Zheng, Z.; Fang, H.; Yang, F.; Liu, Z.-K.; Wang, Y. Amorphous LiLaTiO $_3$  as Solid Electrolyte Material. *J. Electrochem. Soc.* **2014**, *161*, A473–A479.

- (41) Zheng, Z.; Song, S.; Wang, Y. Sol-Gel-Processed Amorphous Lithium Ion Electrolyte Thin Films: Structural Evolution, Theoretical Considerations, and Ion Transport Processes. *Solid State Ionics* **2016**, 287. 60–70.
- (42) Merrill, L. C.; Ford, H. O.; Schaefer, J. L. Application of Single-Ion Conducting Gel Polymers in Magnesium Batteries. *ACS Appl. Energy Mater.* **2019**, *2*, 6355–6363.
- (43) Evans, J.; Vincent, C. A.; Bruce, P. G. Electrochemical Measurement of Transference Numbers in Polymer Electrolytes. *Polymer* 1987, 28, 2324–2328.
- (44) Ma, L.; Fu, C.; Li, L.; Mayilvahanan, K. S.; Watkins, T.; Perdue, B. R.; Zavadil, K. R.; Helms, B. A. Nanoporous Polymer Films with a High Cation Transference Number Stabilize Lithium Metal Anodes in Light-Weight Batteries for Electrified Transportation. *Nano Lett.* **2019**, *19*, 1387–1394.
- (45) Zheng, Z.; Fang, H.-Z.; Liu, Z.-K.; Wang, Y. A Fundamental Stability Study for Amorphous LiLaTiO<sub>3</sub> Solid Electrolyte. *J. Electrochem. Soc.* **2014**, *162*, A244–A248.
- (46) Herstedt, M.; Smirnov, M.; Johansson, P.; Chami, M.; Grondin, J.; Servant, L.; Lassègues, J. C. Spectroscopic Characterization of the Conformational States of the Bis(Trifluoromethanesulfonyl)Imide Anion (TFSI<sup>-</sup>). *J. Raman Spectrosc.* **2005**, *36*, 762–770.
- (47) Li, J.; Zhu, H.; Wang, X.; Macfarlane, D. R.; Armand, M.; Forsyth, M. Increased Ion Conduction in Dual Cation [Sodium] [Tetraalkylammonium] Poly[4 Styrenesulfonyl-(Trifluoromethylsulfonyl)Imide-Co-Ethylacrylate] Ionomers. J. Mater. Chem. A 2015, 3, 19989–19995.
- (48) Ford, H. O.; Park, B.; Jiang, J.; Seidler, M. E.; Schaefer, J. L. Enhanced Li+ Conduction within Single-Ion Conducting Polymer Gel Electrolytes via Reduced Cation—Polymer Interaction. *ACS Mater. Lett.* **2020**, *2*, 272—279.
- (49) Edman, L. Ion Association and Ion Solvation Effects at the Crystalline–Amorphous Phase Transition in PEO–LiTFSI. *J. Phys. Chem. B* **2000**, *104*, 7254–7258.